

# Ionization Quenching Factor measurement of 1 keV to 25 keV protons in Isobutane gas mixture

Benjamin Tampon<sup>1</sup>, Daniel Santos<sup>2</sup>, Olivier Guillaudin<sup>2</sup>, Jean-François Muraz<sup>2</sup>, Lena Lebreton<sup>1</sup>, Thibaut Vinchon<sup>1</sup> and Philippe Querre<sup>3</sup>

<sup>1</sup>*Institut de Radioprotection et de Sûreté Nucléaire (IRSN), PRP-HOM/SDE/LMDN, 13115 Saint Paul Lez Durance, France*

<sup>2</sup>*Laboratoire de Physique Subatomique et de Cosmologie, 38000 Grenoble, France*

<sup>3</sup>*Institut de Radioprotection et de Sûreté Nucléaire (IRSN), PSN-RES/SA2I/LIE, 13115 Saint Paul lez Durance, France*

**Abstract.** The French Institute for Radiation protection and Nuclear Safety (IRSN) is providing reference neutron fluence energy distribution at its standard monoenergetic neutron fields, produced at the AMANDE facility. The neutron energy is assessed by measuring the recoil nuclei energy in a  $\mu$ TPC detector, the LNE-IRSN/MIMAC detector. The knowledge of the ionization quenching factor (IQF) is fundamental to determine the kinetic energy of the recoil nuclei. For some various gases and pressures, discrepancies of about 15% were observed between IQF calculations using the SRIM software and experimental measurements. No data are available for the  $iC_4H_{10} + 50\% CHF_3$  gas mixture which are used for measurements from a few keV up to 565 keV neutron energies in the  $\mu$ TPC detector. The experimental determination of the IQF is of primary importance to provide reference neutron fluence energy distribution. After a short description of the experimental set-up, this paper presents the first results of the IQF measurements in a  $iC_4H_{10} + 50\% CHF_3$  gas mixture in the energy range 1 keV – 25 keV.

## 1 Introduction

The Laboratory for Neutron Metrology and Neutron Dosimetry (LMDN) of the French Institute for Radiation protection and Nuclear Safety (IRSN), is equipped with several neutron facilities. The AMANDE facility, in particular, aims at producing monoenergetic standard neutron fields as recommended by the ISO 8529 [1]. As an associated laboratory to the French National Metrological Institute (LNE), the LMDN has to develop, improve, and maintain the reference quantities associated to its standard neutron fields. To that end, the laboratory has undergone the development of a recoil nuclei-based gas spectrometer, called LNE-IRSN/MIMAC [2], (Micro-tpc MAtRix of Chambers) in order to provide reference values of the neutron fluence, and neutron fluence energy distribution in the energy range of a few keV up to 5 MeV. For the lowest energies, between 8 keV and 565 keV, a  $iC_4H_{10}$  (isobutane) + 50%  $CHF_3$  gas mixture, at 30 and 50 hPa gas pressure, could provide promising results [3][4]. The development of the LNE-IRSN/MIMAC detector is a collaborative effort with the Laboratory of Subatomic Physics and Cosmology (LPSC), which has developed the first MIMAC prototype for directional dark matter search [5].

The neutron fluence energy distribution is determined from the nuclear recoils produced by the neutron elastic scattering in the gas mixture. The neutron energy is determined, event by event, by measuring the scattering angle  $\theta$  and the kinetic energy of the gas nucleus recoil. Preliminary measurements have shown that the recoil nuclei release only a part of their energy through the ionization process. Therefore, the measured energy in the detector does not correspond to the kinetic energy of the recoil nuclei. To assess this quantity, the Ionization Quenching Factor (IQF) has to be determined. The IQF, which is the ratio of the ionization energy and the kinetic energy (Eq. 1), depends on the gas mixture, the pressure, and the energy of the recoil nuclei,

$$IQF = \frac{E_{ionization,ion}}{E_{kinetic,ion}} \quad (1)$$

In the energy range of our interest, and for the chosen gaseous composition, no experimental data are available. The only way to estimate the IQF in our working conditions is to do simulations using SRIM [6] software. To perform experimental measurements of the IQF the LPSC has developed a dedicated facility, called COMIMAC [10].

## 2 The COMIMAC facility

COMIMAC is a table-top ion and electron beams facility, which produces beams in the energy range from few tens of eV up to 50 keV. A picture and a schematic view of the device are shown respectively in Figures 1 and 2. This facility is mainly composed of a COMIC ion source, (Compact Microwave Coaxial) [7], and a measurement chamber. This measurement chamber is a gaseous detector for measuring the ionization energy (Figure 2). A plasma mainly composed of mono-charged ions and electrons is created and maintained in the resonant cavity of the COMIC ion source. Then two electrodes extract and focus the beam. Depending of the polarity and the voltage applied on these electrodes, extracted particles are electrons or ions. A voltage of 1 kV up to 50 kV can be applied to the electrodes, which allows thus the generation of mono-charged beams from 1 keV up to 50 keV. The beam passes then through a micrometric hole [8] which separates the measurement chamber, filled with gas (10 hPa up to 950 hPa), from the ion source, pumped at a secondary vacuum ( $\sim 10^{-5}$  hPa). Once entering in the measurement chamber, the beam's particles lose their energy by ionising the gas. The collection of ionization electron induces an electric current on the anode of a micromegas-type detector [9]. The charges collected on the micromegas are proportional to the ionization energy released in the gas by the particle.



**Figure 1.** Picture of the COMIMAC ion and electron beam generator.

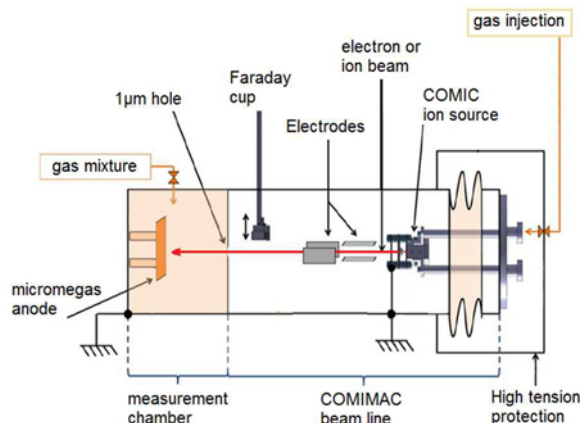


**Figure 2.** Schematic view of the COMIMAC facility.

## 3 IQF measurements in $C_4H_{10}$ + 50% $CHF_3$

### 3.1 Gas purity

The gas used to create the plasma in the COMIC ion source is dihydrogen ( $H_2^a$ ). Despite the high quality of the gas, some impurities are still present. They were mainly coming from air and water outgassing from the one meter long “plastic” pipe, transporting the gas from bottle to the COMIC ion source. The plasma was thus composed of several atoms, including protons which were well identified, as explained in section 4.2.2.

Concerning the gas mixture, the available  $C_4H_{10}^b$  and  $CHF_3^c$  gases were provided and then mixed in the laboratory, in a dedicated buffer volume, as explained later. In case of pollution, electronegative atoms, like oxygen atoms, will capture electrons, and the number of collected charges will be reduced. Therefore, before using the gas mixture, one has to ensure as much as possible, a clean enough chamber and gas pipes. For that, all gas pipes and volumes are preliminary pumped (pressure around  $10^{-5}$  hPa) and gas pipes from bottle to volumes are heated for out-gassing. These precautions allow limiting the gas mixture pollution.

To further limit the pollution, the measurement chamber is completely emptied and then refilled every 4 hours. In this case, the challenge is to keep constant the proportion of both gases in the mixture during the whole measurement campaign. For that, a buffer volume was set up, where gases could be mixed and stored (see Figure 3). A sufficient high quantity of gas mixture is prepared in this buffer at the beginning of the measurement campaign, and then is used to refill the measurement chamber.

<sup>a</sup> Air Liquid -  $H_2$  type N55 - ref P1416S01B0D001

<sup>b</sup> Messer - quality 3.5 ( $iC_4H_{10} > 99.95\%$ )

<sup>c</sup> Air Liquid -  $CHF_3$  type N50 – ref P0737S05R0A001

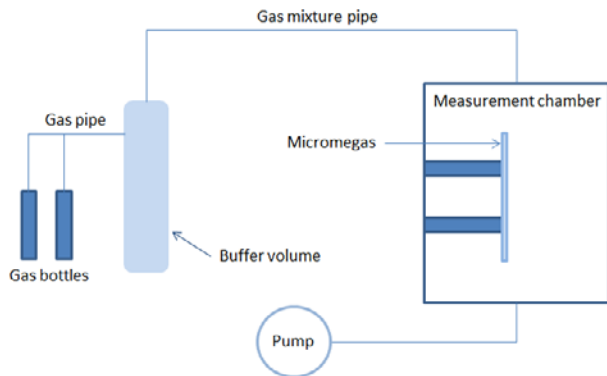


**Figure 3 :** Schematic view of the buffer volume network.

## 3.2 Data acquisition

### 3.2.1 Electronics and acquisition system

The fast electronics as well as the data acquisition software use to perform this experiment has been developed at the LPSC [11]. In the detector, each particle releases its energy by ionizing the gas; this induces a charge current on the grid of the Micromegas [12] which is proportional to the ionization energy deposited. This charge current is then treated by a preamplifier and the output signal is further sent to the FPGA, located on the printed circuit board. The value of the collected charge is recorded and finally sent to the acquisition software. This allows reconstructing for each event a charge collection profile whose amplitude is proportional to the energy deposited by the particle in the detector.

### 3.2.2 Energy calibration

As shown in the Equation 1, the Ionization Quenching Factor depends on the measured ionization energy and the particle kinetic energy. For electrons, in the energy range of 1 keV up to 50 keV, the ionization energy measured corresponds to their kinetic energy, leading to IQF values equal to 1. For that reason, electron beams are ideal to perform the detector energy calibration, as it will be detailed in section 4.2.1.

For a reliable energy calibration, electrons have to lose all their kinetic energy in the active volume of the measurement chamber. This implies that, in our low gas pressure conditions (30 or 50 hPa), only electrons with energy lower than 10 keV can be used.

The other way used to perform the detector energy calibration is to use X-ray sources which are permanently located inside the measurement chamber (see Figure 4). The X-rays interact through photoelectric effect with atoms in the gas. Photoelectrons produced by these interactions lose their kinetic energy by ionizing the gas and electrons are collected by the Micromegas anode. The X-ray sources used are  $^{55}\text{Fe}$  and  $^{109}\text{Cd}$  which produced electrons at 5.92 keV and 3.04 keV respectively [2]. Third electron energy of 1.486 keV, emitted by excited  $^{27}\text{Al}$  atoms, is also used for the calibration. These electrons come from the interaction between the 22 keV

electrons of  $^{109}\text{Cd}$  and the  $^{27}\text{Al}$  present in the detector components.

Once the calibration is performed using these three energy points, the X-ray sources, which are stuck onto a ferrite plate, are moved and hidden behind the Micromegas, by handling a magnet, as shown on Figure 4.

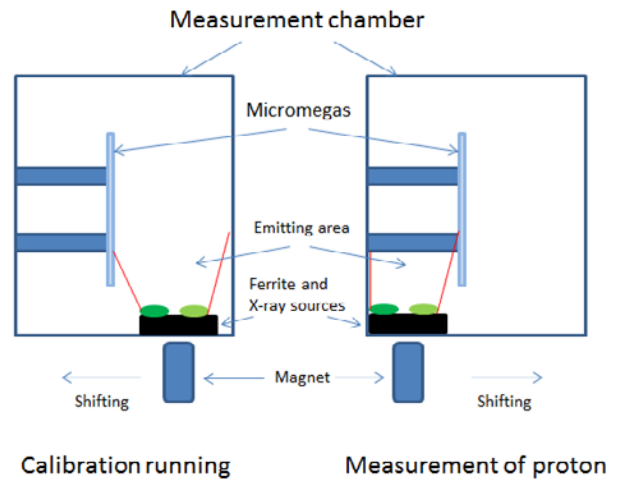


**Figure 4.** Schematic view of measurement chamber with position of X-ray sources.

### 3.2.3 Proton measurements

The kinetic energy of proton beams is determined by the extraction voltage applied on the electrodes see Figure 2. This method has been validated by comparison of X-ray sources with electron beams. In this experimental campaign, measurements were performed for eight different proton energy beams, between 1.5 keV and 25 keV. For each proton beam a minimum of 5000 counts under the proton peak was achieved with a data acquisition time of about 5 minutes each.

### 3.2.4 Monitoring of gas mixture with electrons

Even though all efforts made to keep the pollution as low as possible, as detailed in 3.1, pollution atoms can still be present in the gas mixture. In order to prevent pollution the gas is regularly renewed in the ionization chamber. In addition, during the experiment, the monitoring of the gas mixture degradation is possible by performing frequent energy calibrations. In such a way, one has a quantitative degradation of the gas mixture allowing deciding when the mixture should be renewed.

From this monitoring data, a correction of the Ionization Quenching Factor is computed as a function of this degradation, as it will be explained in section 4.2.3.

## 4 Data analysis

### 4.1 Ballistic effect correction

Due to the charge collection time of the charge preamplifier, which depends on the RC time constant, with  $R = 10 \text{ M}\Omega$  and  $C = 1 \text{ pF}$ , the total charge collection may be reduced. This reduction, called also ballistic effect, is an exponential function expressed as  $\exp(-t/\tau)$  where  $\tau = R \cdot C$ . As a consequence, the measured collected charge does not completely correspond to the ionization energy released by the particles in the detector, which is thus underestimated, as illustrated in Figure 5 for a proton event. In this figure, the experimental collected charge of a proton event (represented by star), which reaches its maximum after about 450 ns, is decreasing with time due the ballistic effect. The second curve represents the collected charge of the same proton if there was no ballistic effect. A correction of this effect is necessary for the determination of the total integration of the collected charges.

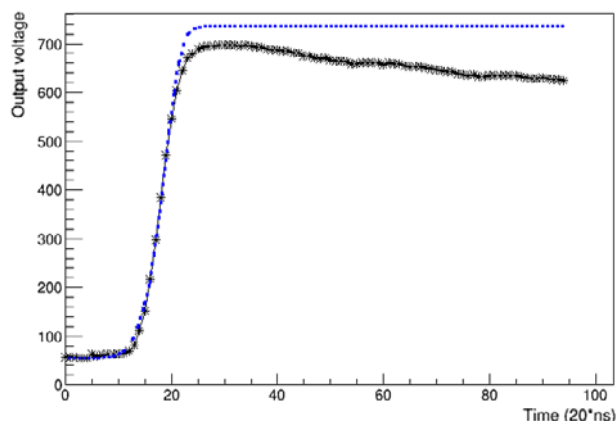


**Figure 5.** Charge collection of a proton event. Black stars is the data measurements and the blue curve represents the ideal charge collection (without ballistic effect).

As explained before, the electronic decreasing is estimated as  $\exp(-t/\tau)$  where  $\tau = R \cdot C$  (with  $R = 10 \text{ M}\Omega$  and  $C = 1 \text{ pF}$ ). The total charge integration of a given event is the difference between the maximum and the minimum values of its charge collection profile. These minimum and maximum values are measured at times  $T_{\min}$  and  $T_{\max}$  (respectively around 0 ns and 450 ns in Figure 5). The time difference  $T$ , given by  $T_{\max} - T_{\min}$  corresponds to the duration of the charge collection of this event. The ballistic effect during this event is  $\exp(-T/\tau)$ , so the associated ballistic correction is  $\exp(+T/\tau)$ .

This ballistic correction has been applied to all events presented hereafter.

### 4.2 Determination of energy

#### 4.2.1 Energy calibration

By analysing each electron event; it is then possible to plot a histogram about the number of events as a function of the integrated charge value measured on the charge preamplifier profile, which corresponds to the ionization energy released in ADC channels. The spectrum of an electron calibration is shown in Figure 6.

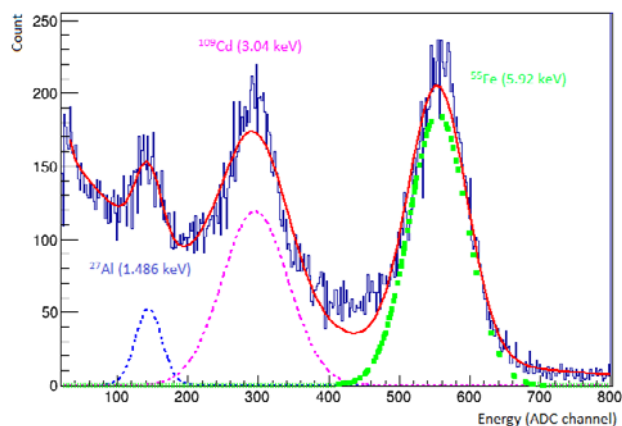


**Figure 6.** Spectrum of calibration running with  $^{55}\text{Fe}$  and  $^{109}\text{Cd}$  in the detector. The red curve is the fit of the spectrum by three Gaussians.

The spectrum shows 3 peaks and a continuum background. The peaks correspond respectively to the three energies of electrons produced by X-rays used to calibrate. The continuum observed is induced by the incomplete collection of electrons with energy greater than 10 keV (like X-ray at 22 keV of  $^{109}\text{Cd}$ ).

The analysis of this spectrum enables to build a calibration curve between ionization energies and ADC channel numbers. In order to determine the parameters associated to this calibration curve, the software MCARE [13] is used. It has been developed by the “Collège Français de Métrologie” and enables computing the equation of a calibration curve with different methods. The most popular is GGMR (General Gauss Markov Regression) which computes the curve parameters with uncertainties on X (number of ADC channel) and Y (energy) as shown on Figure 7.

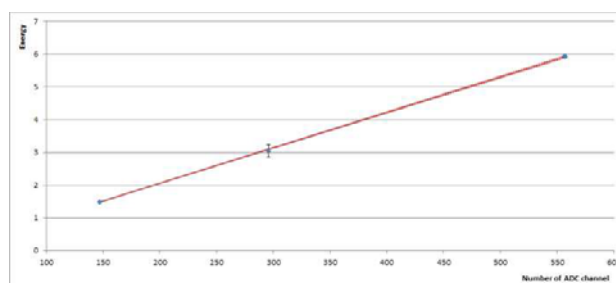


**Figure 7.** Calibration curve built from measurements presented on Figure 6.

Uncertainties of X-ray energies of  $^{27}\text{Al}$ ,  $^{55}\text{Fe}$  and  $^{109}\text{Cd}$  are taken from ENDF VII.1 data base. Indeed, the measurement of the energy mean (1,486 keV and 3,04 keV and 5,92 keV) and the uncertainty associated (0,01

keV and 0,2 keV and 0,04 keV respectively) are realized with the probability distribution of X-ray for these three energies.

As explained before, the software MCARE allows calculating parameters for the energy calibration curve. Moreover, it gives the uncertainty associated to each point on the curve too. This is needed to perform the calculation of uncertainty on IQF measurements, as it will be explained in section 5.

#### 4.2.2 IQF measurements

The same kind of spectrum shown for electrons is created for proton events. In Figure 8 is presented the spectrum obtained for the protons with a kinetic energy of 25 keV.

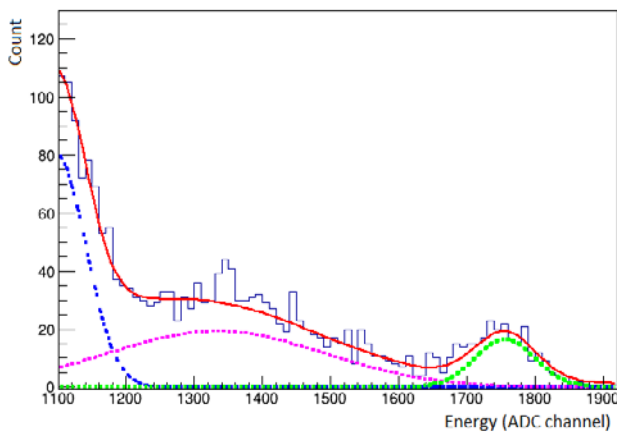


**Figure 8.** Spectrum obtained for a proton beam with 25 keV kinetic energy. The red line corresponds to the fit of the spectrum. The green Gaussian fit is the proton peak and the two other Gaussians are peaks of pollutions (other nuclei at 25 keV kinetic energies).

On a given spectrum for protons, there are, in general, several well-defined peaks, which correspond to atoms present in the gas constituting the plasma in the ion source, see section 2. These peaks are even more important when a Wien filter is not used, as it was the case for these measurements. Whatever the ionization energy of the particle, the proton peak is always at the highest ionization energy. This is because the quenching in ionization increases with the mass of the atoms. This means that heavier the atoms smaller are their IQF. According to equation 1, the heavier than the proton atoms have smaller released ionisation energy than the proton. That property explains that protons, which are the lightest elements, will be always on the right of spectra.

In Figure 8, the spectrum obtained with a 25 keV proton beam is shown. The position of the proton peak, which is the mean of the Gaussian, was combined with the energy calibration on MCARE to determine the ionisation energy released by protons at this energy. Then, according to the equation 1, the Ionisation Quenching Factor could be calculated.

Uncertainties associated to these IQF measurements for each energy were calculated from the uncertainty of the proton peak and the ionisation energy released (related to the energy calibration uncertainties like

explained in part 4.2.1). The proton peak is assumed to be a Gaussian so the associated uncertainty was  $\sigma/(N)^{1/2}$ , where sigma is normalized by the mean and N is the number of events issued from the Gaussian curve integral.

As explained in 3.2, energy calibrations are repeated before and after each measurement of protons at different energies to monitor the degradation of the gas mixture. In order to correct this degradation, a linear interpolation is realized for each proton measurement. After the calculations of IQF for the two energy calibrations (performed just before and after this measurement), the corrected IQF is defined as the linear combination function of time of the two calibrations and of the time of the proton measurement.

**Table 1.** Notation definitions for IQF interpolation.

| Measurements  | Time | IQF (t1) | IQF(t2) | IQF(t) |
|---------------|------|----------|---------|--------|
| Calibration 1 | t1   |          |         |        |
| proton        | t    | IQF1     | IQF2    | IQF    |
| Calibration 2 | t2   |          |         |        |

In the situation described in **Table 1**, the interpolated value of IQF will be:

$$IQF = \frac{\left(\frac{t-t_1}{t_2-t_1} * IQF_2 + \frac{t_2-t}{t_2-t_1} * IQF_1\right)}{2} \quad (2)$$

With this method, the gas degradation is no longer an issue for the measurement of IQF, as long as a linear degradation of the gas can be assumed.

## 5 Results

Before this experiment, no experimental data on Ionization Quenching Factors were available in literature in our energy range of interest. As seen in the section 1, the only way to estimate the IQF was to use the SRIM simulation software. In Figure 9 are presented the IQF values as a function of proton energy in a 50% C<sub>4</sub>H<sub>10</sub> + 50% CHF<sub>3</sub> gas mixture, computed by SRIM simulation in red and those deduced from the data obtained during this experimental campaign.

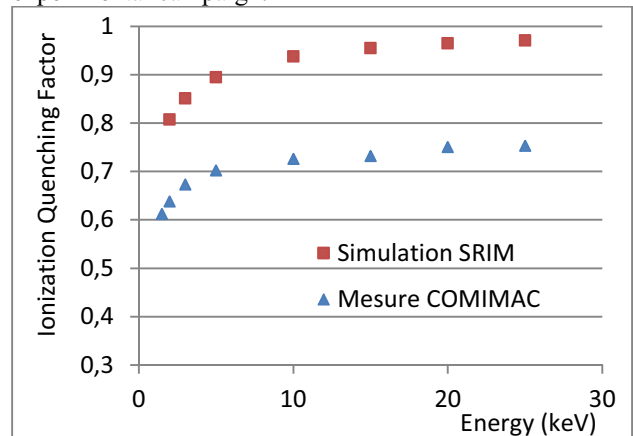


**Figure 9.** IQF measurements.

Uncertainties of experimental data are not visible on the Figure 9 because they do not exceed 0,01, which correspond to 1.16% of uncertainties at 1.5 keV.

The COMIMAC facility allows measuring the Ionization Quenching Factor of a gas mixture in-situ taking into account the pollution in the chamber with low uncertainties. These results will become the reference for the IQF of proton in 50% C<sub>4</sub>H<sub>10</sub> + 50% CHF<sub>3</sub> gas mixture at 50 mbar. The IQF depends on the amount of pollution and on the pressure of the gas. Indeed, the SRIM simulations on the Ionization Quenching Factor do not show this dependency on the gas pressure. The SRIM simulation, shown in figure 8, overestimates the IQF of protons in this case. This difference represents the limitations of SRIM calculations on the IQF estimation in this low energy range. Indeed, this software is only optimized and validated for calculations around a few MeV per nucleon when this work concerns energies around a few keV.

It is theoretically expected that at higher energies the IQF will be closer than 1. But it appears that the limitations in the energy range of COMIMAC ( $E < 50$  keV) prevent to explore the IQF in the MeV range. However, for fast neutron fields characterization in the MeV range an exploration of the IQF in such a range of energy will be performed in a future work.

### Acknowledgement

This work is partially funded by the French National Metrology Institute (LNE) under contract LNE/DRST 15 7 004.

### Bibliography

- [1] International Organization for standardization 2001 *Reference Neutron Radiations - Part 1: Characteristics and methods of production* ISO8529-1
- [2] D. Maire, *Développement d'une chambre à projection temporelle utilisant une anode pixélisée pour les références en énergie et en fluence de champs neutroniques de basses énergies (quelques keV à 5 MeV)*, PhD Thesis (in french) (2015).
- [3] C. Golabek et al., *A  $\mu$ TPC detector for the characterization of low energy neutron fields*, NIM A, vol. 678, pp. 33-38. 2012.
- [4] D. Maire et al., *Development of a  $\mu$ TPC detector as a standard instrument for low energy neutron field characterization*, Rad. Prot. Dos., vol. 161, Nos 1-4, pp. 245-248, 2014.
- [5] D. Santos et al., *MIMAC, Micro-tpc Matrix of Chambers for dark matter directional detection*, Proceedings of the 4th International Conference on Directional Dark Matter Detection CYGNUS2013, held in Toyoma (Japan), 2013.
- [6] J.F. Ziegler et al., *SRIM – The stopping and range of ions in matter (2010)*, NIM B 268 (2010) 1818-1823.
- [7] P. Sortais et al., *Ultra compact / Ultra low power ECRIS for multi-purpose applications*, Rev. Sci. Instrum. 81, 02B314, 2010.

[8] D. Santos et al., *Ionization Quenching Factor Measurement of  $^4\text{He}$* , arXiv :0810.1137v1.

[9] I. Giomataris et al., *Micromegas in a bulk*, NIM A, vol. 560, pp. 405-408, 2006.

[10] J.F. Muraz et al., *A table-top ion and electron beam facility for ionization quenching measurement and gas detector calibration*. NIM A 832 (2016) 214-218

[11] O. Guillaudin et al., *Quenching factor measurement in low pressure gas detector for directional dark matter search*, arXiv:1110.2042v1

[12] G.F. Knoll. *Radiation and Measurement Third Edition*, Wiley and sons, 2000

[13] M-CARE v1.0: C4GH10, retrieved 20/12/2014.